

Limitations of SVD-Based Diagnostics for Non-Hermitian Many-Body Localization with Time-Reversal Symmetry

Huimin You,¹ Jinghu Liu,² Yunbo Zhang,^{3,*} and Zhihao Xu^{1,†}

¹*Institute of Theoretical Physics and State Key Laboratory of Quantum Optics Technologies and Devices, Shanxi University, Taiyuan 030006, China*

²*Department of Physics, Xinzhou Normal University, Xinzhou, Shanxi 034000, China*

³*Zhejiang Key Laboratory of Quantum State Control and Optical Field Manipulation, Department of Physics, Zhejiang Sci-Tech University, Hangzhou 310018, China*

(Dated: February 10, 2026)

Singular value decomposition (SVD) has been used to construct Hermitian-like diagnostics for non-Hermitian many-body systems, but its reliability for identifying many-body localization (MBL) transitions—particularly in time-reversal-symmetry (TRS) preserving settings—remains unclear. Here we benchmark SVD-based diagnostics against exact diagonalization (ED) in TRS-preserving non-Hermitian hard-core-boson chains with nonreciprocal hopping, considering three representative potentials: a quasiperiodic potential, random disorder, and a Stark potential. We compare spectral statistics, half-chain entanglement entropy, inverse participation ratio, and spectral form factors. For the quasiperiodic and random-disorder models, ED yields mutually consistent transition estimates, whereas SVD systematically shifts the inferred critical disorder strength to larger values and can lead to different phase assignments. In contrast, for the clean Stark model ED and SVD locate a consistent critical tilt. Our results show that while SVD-based diagnostics capture qualitative trends, they are not generically reliable for quantitatively locating the MBL transition in TRS-preserving non-Hermitian many-body systems.

PACS numbers:

I. INTRODUCTION

Many-body localization (MBL) is widely viewed as a paradigmatic mechanism by which an interacting system can avoid thermalization in the presence of strong disorder [1, 2]. Unlike Anderson localization, which applies to noninteracting particles, MBL can remain stable even when interactions are present [3]. Consequently, the thermal-to-MBL transition is often discussed as a dynamical transition from an ergodic (thermalizing) regime to a localized, nonergodic regime [4–8]. Standard diagnostics in Hermitian systems include spectral and eigenstate properties: level statistics typically cross over from Wigner-Dyson to Poisson [3, 9], and eigenstate entanglement changes from volume-law scaling to area-law-like behavior [10]. A useful theoretical framework is provided by local integrals of motion (LIOMs), which explains the absence of transport and the persistence of memory at long times [11–13].

In recent years, there has been growing interest in extending these ideas to open quantum systems and non-Hermitian settings, where effective non-Hermitian Hamiltonians can arise, for example in quantum-trajectory dynamics conditioned on no quantum jumps [14–19]. A difficulty is that non-Hermitian Hamiltonians generally have complex eigenvalues, which complicates the use of standard spectral tools developed for Hermitian problems

[20–23]. To address this issue, several works have advocated the use of singular value decomposition (SVD), since singular values are always real and non-negative [24, 25]. This makes it possible to define Hermitian-like diagnostics, such as singular-value spacing ratios [26] and the singular form factor (σ FF), while keeping the numerical analysis straightforward. For instance, Ref. [27] applied singular-value statistics, σ FF, and properties of singular vectors to diagnose transitions between random-matrix theory (RMT)-like [28–31] and Poisson-like behavior in an interacting spin chain with random local dissipation. Notably, most SVD-based numerical studies have focused on non-Hermitian models that break time-reversal symmetry (TRS), while the TRS-preserving case remains less explored from the SVD perspective. Here TRS denotes an antunitary symmetry \mathcal{T} implemented as complex conjugation, satisfying $\mathcal{T}\hat{H}\mathcal{T}^{-1} = \hat{H}$ for the TRS-preserving models considered below. We therefore ask whether SVD-based diagnostics can faithfully locate the MBL transition in TRS-preserving non-Hermitian systems.

At the same time, the agreement between SVD- and exact diagonalization (ED)-based diagnostics is not guaranteed, as has been demonstrated primarily in TRS-breaking non-Hermitian settings. In particular, Ref. [32] showed that, depending on the model and disorder type, ED and SVD can place the transition in different parameter regimes. Similar SVD-based analyses have also been applied to chaos-to-nonchaos crossovers in other TRS-breaking non-Hermitian models, including non-Hermitian Sachdev-Ye-Kitaev and random-matrix ensembles [33, 34]. Here we shift the focus to a distinct

*Electronic address: ybzhang@zstu.edu.cn

†Electronic address: xuzhihao@sxu.edu.cn

question: whether SVD-based diagnostics remain reliable in TRS-preserving non-Hermitian many-body systems, where their applicability has not been systematically assessed. To this end, we perform a side-by-side comparison between ED- and SVD-based probes, including spacing ratios [35–38], half-chain entanglement entropy [39, 40], inverse participation ratio (IPR) [41, 42], and spectral form factors (SFFs) [43–45]. This allows us to delineate parameter regimes where the two approaches agree or disagree in classifying ergodic-like versus MBL-like behavior in TRS-preserving models.

TRS can play a crucial role in non-Hermitian many-body systems, but it has been less emphasized in the existing SVD-based literature. In disordered non-Hermitian systems preserving TRS, the spectrum often exhibits a real-to-complex transition that is frequently discussed in connection with the MBL transition [46, 47]. By contrast, when TRS is broken, such a spectral transition is generally absent, even if MBL persists [47]. However, TRS alone does not ensure that spectral and MBL transitions coincide: in the TRS-preserving interacting Stark model, the Stark-MBL transition and the real-to-complex spectral transition occur at parametrically different tilt strengths [48]. These observations motivate us to examine, in TRS-preserving non-Hermitian systems, when SVD-based diagnostics are consistent with ED-based indicators of the MBL transition, and to delineate the regimes in which they may deviate.

In this work, we combine ED with SVD to systematically assess the range and limitations of SVD-based diagnostics in TRS-preserving non-Hermitian many-body systems. We study three representative hard-core-boson chains subject to (i) a quasiperiodic potential, (ii) random disorder, and (iii) a Stark potential. In all three settings, the Hamiltonian can be written as $\hat{H} = \hat{H}_I + \hat{W}$, where

$$\hat{H}_I = \sum_j \left[-J \left(e^{-g} \hat{b}_{j+1}^\dagger \hat{b}_j + e^g \hat{b}_j^\dagger \hat{b}_{j+1} \right) + U \hat{n}_j \hat{n}_{j+1} \right], \quad (1)$$

and $\hat{W} = \sum_j W_j \hat{n}_j$ encodes the model-dependent on-site potential. Here, \hat{b}_j (\hat{b}_j^\dagger) annihilates (creates) a hard-core boson on site j , and $\hat{n}_j = \hat{b}_j^\dagger \hat{b}_j$ is the local number operator. The parameter J sets the hopping amplitude, and U is the nearest-neighbor interaction strength. Non-Hermiticity is introduced via non-reciprocal hopping controlled by g . For $g \neq 0$, left and right hopping amplitudes differ by factors $e^{\mp g}$. We directly compare ED- and SVD-based indicators at the level of both eigenstate properties and spectral correlations. This comparison allows us to identify regimes where SVD diagnostics remain consistent with ED-based indicators of the MBL transition. Within ED, the n th eigenvalue and the corresponding right eigenstate are denoted by E_n and $|\psi_n\rangle$, respectively. In the SVD framework, $\hat{H} = U \Sigma V^\dagger = \sum_n \sigma_n |u_n\rangle \langle v_n|$, where $U = (|u_1\rangle, \dots, |u_D\rangle)$ and $V = (|v_1\rangle, \dots, |v_D\rangle)$ are the left and right singular vectors, respectively, and $\Sigma = \text{diag}(\sigma_1, \dots, \sigma_D)$ contains the singular values. We

denote the n th singular value and the corresponding right singular vector by σ_n and $|v_n\rangle$, respectively. Unless stated otherwise, we work at half filling $N/L = 1/2$, where N is the particle number and L is the system size; the corresponding Hilbert-space dimension is $D = \binom{L}{N}$. For cases (i) and (ii), all quantities are averaged over disorder realizations and, for each realization, over a fixed bulk spectral window; throughout, the bulk window is taken to be the central one-fifth of the spectrum. For the Stark case (iii), where no disorder ensemble is present, we restrict to the same bulk spectral average only.

We characterize spectral correlations using the level-spacing ratio, a standard diagnostic in quantum chaos and RMT that quantifies level repulsion and thus distinguishes RMT-like from Poisson-like spectral correlations. For the complex spectrum obtained from ED, we employ the complex spacing ratio [32, 49–51]

$$z_n = \frac{E_n - E_{\text{NN}}}{E_n - E_{\text{NNN}}} = |z_n| e^{i\varphi_n}, \quad (2)$$

where E_{NN} and E_{NNN} are the nearest and next-nearest neighbors of E_n in the complex-energy plane, respectively. Here “nearest” is determined by the Euclidean distance $|E_m - E_n|$ in the complex plane, and $|z_n|$ and φ_n are the magnitude and argument of z_n . We define the disorder- and bulk-spectrum-averaged radial statistic as $\langle r^E \rangle = \langle |z| \rangle$, where $\langle \dots \rangle$ indicates an average over eigenvalues in the chosen bulk window and over disorder realizations. In non-Hermitian systems, $\langle r^E \rangle$ typically approaches the Ginibre (RMT-like) value $\langle r^E \rangle \approx 0.74$ in regimes with strong spectral correlations, whereas it tends to the Poisson value $\langle r^E \rangle \approx 0.5$ when spectral correlations are weak [49, 50, 52]. Within the SVD framework, the singular values form a real, non-negative spectrum. We order them in ascending order, and use the conventional spacing ratio [3, 53]

$$r_n = \frac{\min(\delta_{n+1}, \delta_n)}{\max(\delta_{n+1}, \delta_n)}, \quad (3)$$

with the nearest-neighbor spacing $\delta_n = \sigma_{n+1} - \sigma_n$. The corresponding disorder- and bulk-spectrum average is denoted by $\langle r^S \rangle = \langle r \rangle$ [27, 32]. When the singular-value spectrum exhibits RMT-like correlations, $\langle r^S \rangle$ approaches the Gaussian orthogonal ensemble (GOE) value $\langle r^S \rangle \approx 0.53$, while it crosses over to the Poisson value $\langle r^S \rangle \approx 0.39$ in the weakly correlated regime [3, 54]. Comparing $\langle r^E \rangle$ and $\langle r^S \rangle$ allows us to diagnose whether spectral correlations are RMT-like or Poisson-like, while the nature of the underlying eigenstates (extended/ergodic versus localized/MBL) is assessed in conjunction with entanglement entropy and IPR.

Entanglement entropy provides a key quantity for characterizing the MBL transition. We consider the half-chain von Neumann entanglement entropy of the n th state [49, 55]

$$S_n = -\text{Tr}(\rho_A^n \ln \rho_A^n), \quad (4)$$

where the system is bipartitioned into two equal subsystems A and B with $L_A = L_B = L/2$. The reduced density matrix $\rho_A^n = \text{Tr}_B(\rho^n)$ is obtained by tracing out subsystem B . In the ED approach, we construct the density matrix from the n th right eigenstate as $\rho^n = |\psi_n\rangle\langle\psi_n|$. In the SVD approach, we analogously define $\rho^n = |v_n\rangle\langle v_n|$ using the n th right singular vector v_n [27]. We denote the disorder- and bulk-spectrum-averaged half-chain entanglement entropies extracted from ED and SVD by $\langle S^E \rangle$ and $\langle S^S \rangle$, respectively. The scaling of entanglement entropy with system size distinguishes extended and localized eigenstates [56]. In extended/ergodic regimes, the entanglement entropy exhibits volume-law scaling, consistent with highly entangled states. In localized/MBL-like regimes, it approaches an area-law-like scaling, reflecting reduced entanglement [12].

Complementary to spectral and entanglement diagnostics, we further characterize the spatial distribution properties of the states via the IPR, which quantifies how localized a normalized state is in a chosen basis. For a Hilbert space dimension D , the IPR of the n th state is defined as [12, 49, 57]

$$\text{IPR}_n = \sum_{k=1}^D |c_k|^4, \quad (5)$$

where c_k are the expansion coefficients in the computational basis $\{|e_k\rangle\}$. In the ED approach, $c_k^E = \langle e_k | \psi_n \rangle$, while in the SVD approach we analogously define $c_k^S = \langle e_k | v_n \rangle$ using the right singular vector $|v_n\rangle$ [27, 32]. The IPR distinguishes localized and extended structures: in a strongly localized phase, $\text{IPR}_n = O(1)$, whereas for a fully extended state one expects $\text{IPR}_n = O(1/D)$ [27]. Accordingly, we denote the disorder- and bulk-spectrum-averaged IPR obtained from ED and SVD by $\langle \text{IPR}^E \rangle$ and $\langle \text{IPR}^S \rangle$, respectively.

We also study SFFs, which probe long-range spectral correlations in the time domain and provide a sensitive diagnostic of RMT-like versus Poisson-like behavior. For the complex energy spectrum $\{E_n\}$ obtained from ED, we use the dissipative SFF (DSFF) [58, 59]

$$\text{DSFF}(\tau, \tau^*) = \left| \frac{1}{D} \sum_{n=1}^D \exp \left[\frac{i}{2} (E_n \tau^* + E_n^* \tau) \right] \right|^2, \quad (6)$$

where $\tau = te^{i\theta}$ defines a complex “time” variable. τ is a Fourier-conjugate parameter to the real and imaginary parts of the complex spectrum rather than the physical real time of unitary dynamics. We take $\theta \in [0, \pi/2]$ and fix $\theta = \pi/4$ throughout, which treats the real and imaginary parts on equal footing and is appropriate for generic complex spectra. Within the SVD approach, we consider the σ FF defined in terms of the unfolded singular values $\{\tilde{\sigma}_n\}$, which are obtained by mapping the singular values of the non-Hermitian Hamiltonian through a standard unfolding procedure based on a smooth fit to the cumulative distribution function [60], thereby ensuring that

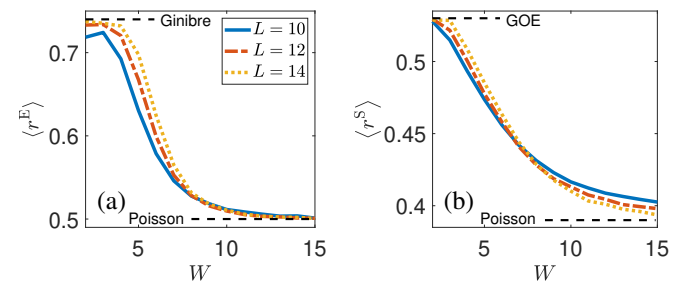


FIG. 1: Disorder-averaged spacing ratios (a) $\langle r^E \rangle$ and (b) $\langle r^S \rangle$ versus quasiperiodic potential strength W for different system sizes. Dashed lines indicate the corresponding RMT and Poisson reference values.

global density variations do not contaminate the correlation measures [27, 34, 61–66]

$$\sigma\text{FF}(t) = \left| \frac{1}{D} \sum_{n=1}^D e^{-i\tilde{\sigma}_n t} \right|^2. \quad (7)$$

This quantity plays a role analogous to the conventional SFF in Hermitian systems, but is constructed from the real, non-negative singular spectrum. In regimes with RMT-like spectral correlations, DSFF and $\sigma\text{FF}(t)$ exhibit the characteristic dip–ramp–plateau structure and approach the corresponding RMT predictions. In Poisson-like regimes, the ramp is strongly suppressed. Therefore, together with level spacing ratios and eigenstate-based measures, DSFF and σFF provide additional diagnostics for distinguishing RMT-like from Poisson-like behavior.

In this paper, we set $J = 1$ as the energy unit and fix the parameters to $U = 2$ and $g = 0.5$. All calculations are performed under periodic boundary conditions. For both the quasiperiodic and random models, we average over 8000, 3000, and 200 independent realizations for $L = 10, 12$, and 14, respectively.

II. QUASI-PERIODIC MODEL

We consider a TRS-preserving non-Hermitian hardcore-boson chain subject to a quasiperiodic on-site potential, $W_j = W \cos(2\pi\alpha j + \phi)$, where W is the potential strength and $\phi \in [0, 2\pi]$ is a random phase. We choose an irrational modulation wave number $\alpha = (\sqrt{5} - 1)/2$.

To diagnose an ergodic-to-MBL transition, we compare spectral-statistics diagnostics obtained from ED and SVD. We first evaluate the level-spacing ratio defined in Eq. (2) using the complex many-body eigenvalues. As shown in Fig. 1(a), $\langle r^E \rangle$ is close to Ginibre value at weak quasiperiodic potential and gradually drifts toward the Poisson limit as W increases, indicating a transition from an ergodic regime to a MBL regime. We then repeat the analysis in the SVD framework by computing the spacing ratio defined in Eq. (3) for the singular values. Fig-

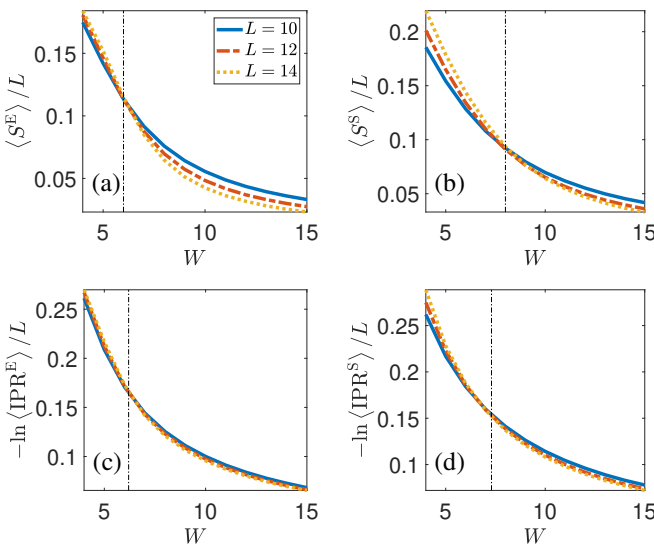


FIG. 2: Half-chain entanglement entropy and IPR versus quasiperiodic strength W for different system sizes. Entanglement: (a) $\langle S^E \rangle$ and (b) $\langle S^S \rangle$. IPR: (c) $\langle \text{IPR}^E \rangle$ and (d) $\langle \text{IPR}^S \rangle$. Dashed lines mark the critical points from finite-size scaling.

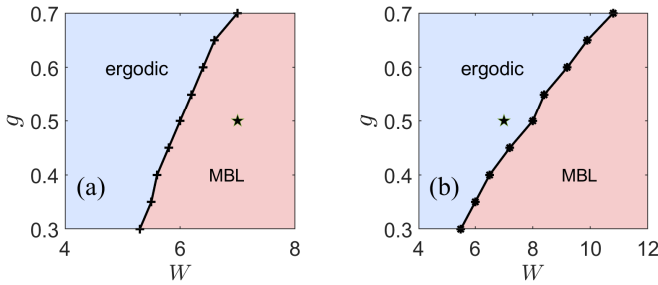


FIG. 3: Phase diagram of the quasiperiodic model in the (g, W) plane. (a) ED boundary extracted from $\langle S^E \rangle$. (b) SVD boundary extracted from $\langle S^S \rangle$. The marked point indicates the representative parameters $(g, W) = (0.5, 7)$.

ure 1(b) shows a similar drift of $\langle r^S \rangle$ from an RMT-like value toward the Poisson limit.

To locate the transition more accurately, we further analyze the half-chain entanglement entropy. In the ergodic regime, the entanglement entropy exhibits volume-law scaling, whereas in the MBL regime it crosses over to an area-law-like behavior [12]. Concretely, we compute the phase- and bulk-spectrum-averaged half-chain entanglement entropies $\langle S^E \rangle$ and $\langle S^S \rangle$ for three system sizes, with the results shown in Fig. 2(a) and Fig. 2(b), respectively. The finite-size scaling collapse in Fig. 2(a) yields an ED-based transition estimate $W_c^E \approx 6$. By contrast, the corresponding collapse in Fig. 2(b) places the SVD-based transition at a substantially larger value, $W_c^S \approx 8$. This systematic shift indicates that, in this TRS-preserving quasiperiodic non-Hermitian setting, the SVD-based en-

tanglement diagnostic does not reliably track the ED-inferred transition point.

As an independent check, we compute the IPR for both approaches. Specifically, we evaluate $\langle \text{IPR}^E \rangle$ and $\langle \text{IPR}^S \rangle$ for the same three system sizes, which are shown in Fig. 2(c) and Fig. 2(d). Consistent with the entanglement analysis, both quantities increase with W and display a size-dependent crossover toward stronger localization. The finite-size scaling collapse yields $W_c^E \approx 6.2$ from $\langle \text{IPR}^E \rangle$ and $W_c^S \approx 7.3$ from $\langle \text{IPR}^S \rangle$. The persistence of an ED-SVD mismatch across two independent observables suggests that the discrepancy is not an artifact of a particular diagnostic, but rather reflects that singular-vector-based measures are not reliable for quantitatively locating the transition in this TRS-preserving quasiperiodic non-Hermitian model.

To provide an intuitive overview, we summarize these results in the phase diagrams shown in Fig. 3. Figure 3(a) displays the ED-based phase diagram extracted from the half-chain entanglement entropy, where the solid line marks the transition boundary separating an ergodic phase from a MBL phase in the (g, W) plane. Figure 3(b) presents the corresponding SVD-based phase diagram obtained from the same entanglement criterion. Although the two phase diagrams share a similar overall structure, the SVD-based boundary is systematically shifted to larger W . Importantly, this shift can lead to a qualitative misclassification of the phase at the same point in parameter space. As a representative example, the point $(g, W) = (0.5, 7)$ in Fig. 3 lies on the localized side of the ED-based boundary, while it is still identified as ergodic by the SVD-based boundary, directly highlighting that the SVD approach is not reliable for determining the phase boundary in this TRS-preserving quasiperiodic non-Hermitian setting.

Finally, we employ DSFF and σ FF to probe the spectral correlations in the time domain across the transition region, as shown in Figs. 4(a) and 4(b), respectively. Both quantities are computed for $L = 14$ and average over 200 realizations of the random phase ϕ . In Fig. 4(a), the DSFF at $W = 7$ and $W = 15$ shows no discernible ramp, indicating Poisson-like behavior. In contrast, Fig. 4(b) shows that the σ FF at $W = 4$ exhibits the characteristic dip-ramp-plateau structure [27, 34], indicating level repulsion consistent with RMT and hence an ergodic phase. At the intermediate value $W = 7$, a ramp is still visible in σ FF but is suppressed, while the DSFF remains Poisson-like. This difference between DSFF and σ FF at the same parameter point provides dynamical support that in TRS-preserving quasiperiodic non-Hermitian systems, SVD-based diagnostics can yield inconsistent transition classifications and are therefore not reliable for pointing the ergodic-to-MBL transition.

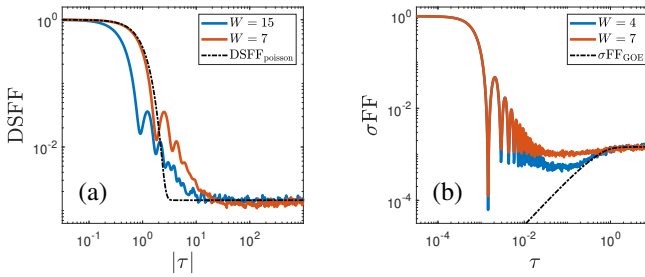


FIG. 4: Dynamics of the DSFF and σ FF for the quasiperiodic model at $L = 14$, averaged over 200 realizations. (a) DSFF for $W = 7$ and 15; the dashed line marks the Poisson behavior. (b) σ FF for $W = 4$ and 7; dashed lines show the GOE predictions.

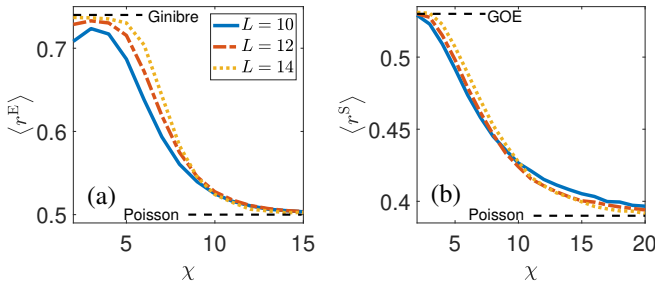


FIG. 5: Disorder-averaged spacing ratios (a) $\langle r^E \rangle$ and (b) $\langle r^S \rangle$ versus random disorder strength χ for different system sizes L . Dashed lines denote the corresponding RMT and Poisson reference values.

III. RANDOM-DISORDERED MODEL

We next turn to the TRS-preserving non-Hermitian hard-core-boson chain with random on-site disorder. The Hamiltonian is the same as in Eq. (1), with the on-site potential term now taken to be a random disorder potential. Specifically, W_j is drawn independently from a uniform distribution, $W_j \in [-\chi, \chi]$, where χ controls the disorder strength. All other parameters and numerical protocols are chosen identically to those used in the quasiperiodic model, enabling a direct ED–SVD comparison in the TRS-preserving random disordered setting.

We first characterize spectral correlations using spacing-ratio statistics. From ED, we compute the complex spacing-ratio $\langle r^E \rangle$ from the complex many-body eigenvalues. As shown in Fig. 5(a), $\langle r^E \rangle$ evolves from a Ginibre-like value at weak disorder toward the Poisson limit as χ increases, signaling an ergodic-to-MLB transition. In the SVD framework, the singular-value spacing ratio $\langle r^S \rangle$ in Fig. 5(b) exhibits a corresponding drift from a GOE-like value toward Poisson statistics.

To locate the transition, we next analyze state-based diagnostics. Figures 6(a) and 6(b) show the disorder- and bulk-spectrum-averaged half-chain entanglement entropies $\langle S^E \rangle$ and $\langle S^S \rangle$ for three system sizes. With in-

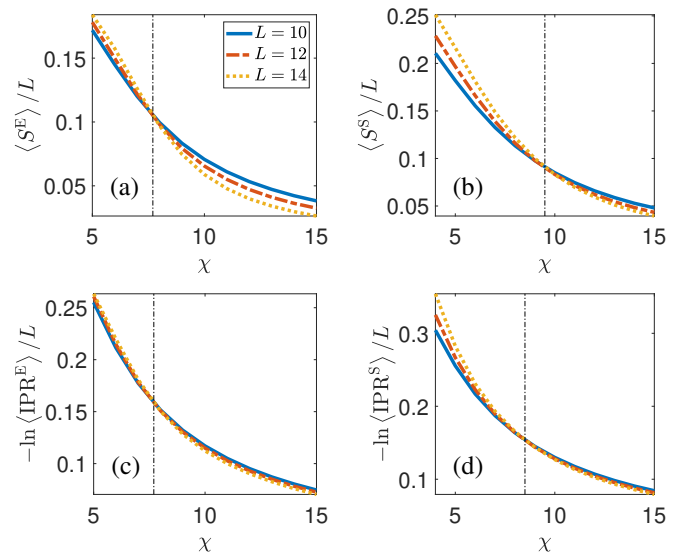


FIG. 6: Half-chain entanglement entropy and IPR versus random disorder strength χ for different system sizes L . Entanglement: (a) $\langle S^E \rangle$ and (b) $\langle S^S \rangle$. IPR: (c) $\langle \text{IPR}^E \rangle$ and (d) $\langle \text{IPR}^S \rangle$. Dashed lines mark critical points from finite-size scaling.

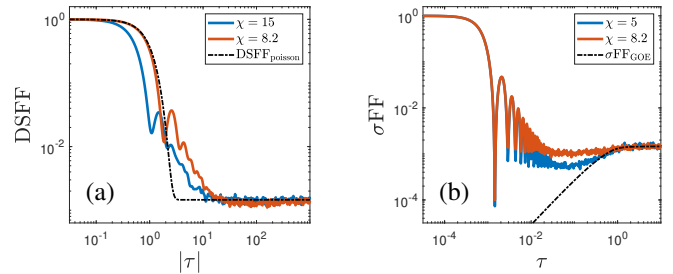


FIG. 7: Dynamics of the DSFF and σ FF for the random-disorder model at $L = 14$, averaged over 200 disorder realizations. (a) DSFF for $\chi = 8.2$ and 15; the dashed line indicates the Poisson behavior. (b) σ FF for $\chi = 8.2$ and 5; the dashed line shows the GOE prediction.

creasing χ , both entropies decrease, reflecting a crossover from volume-law scaling to an area-law-like behavior. The finite-size scaling collapse, however, yields markedly different critical disorders. In Fig. 6(a), an ED-based transition estimate is $\chi_c^E \approx 7.7$, whereas Fig. 6(b) places the SVD-based transition at a significantly larger value, $\chi_c^S \approx 9.5$.

We further test this discrepancy using the IPR. From Figs. 6(c) and 6(d), the scaling collapses yield $\chi_c^E \approx 7.7$ from $\langle \text{IPR}^E \rangle$ and $\chi_c^S \approx 8.5$ from $\langle \text{IPR}^S \rangle$. Therefore, the ED-based transition points extracted from entanglement and IPR are mutually consistent, while the SVD-based estimates are not only shifted to larger disorder but also show a stronger observable dependence. This systematic ED–SVD mismatch indicates that, in the present

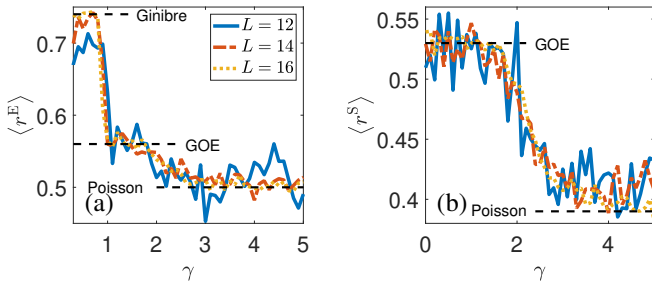


FIG. 8: Disorder-averaged spacing ratios (a) $\langle r^E \rangle$ and (b) $\langle r^S \rangle$ versus Stark tilt γ for different system sizes. Dashed lines denote the corresponding RMT and Poisson reference values: Ginibre/GOE/Poisson in (a) and GOE/Poisson in (b).

TRS-preserving random-disorder non-Hermitian model, SVD-based diagnostics are not reliable for quantitatively determining the MBL transition.

Finally, we test whether the ED–SVD mismatch also appears in SFFs. We choose an intermediate disorder strength $\chi = 8.2$, lying between χ_c^E and χ_c^S , and compute the DSFF and σ FF at $L = 14$, averaged over 200 disorder realizations in Fig. 7. In Fig. 7(a), the DSFF at $\chi = 8.2$ shows no discernible ramp, resembling the strongly disordered case $\chi = 15$, which is indicative of Poisson-like spectral correlations in the ED picture. In contrast, Fig. 7(b) shows that the σ FF at the same $\chi = 8.2$ still exhibits a weak ramp, and at weaker disorder (e.g., $\chi = 5$) it develops a clear dip–ramp–plateau structure, characteristic of an ergodic regime in the SVD picture. Therefore, at the same point $\chi = 8.2$, DSFF and σ FF lead to different conclusions. Together with the shifted SVD critical points in Fig. 6, this shows that in TRS-preserving non-Hermitian systems the SVD-based diagnostics can misplace the transition and misidentify the phase, and hence are not reliable for determining the MBL transition in the random-disorder model.

IV. STARK MODEL

We now turn to a clean TRS-preserving non-Hermitian hard-core-boson chain in a Stark potential. The on-site potential is $W_j = -\gamma(j-1) + \beta \left(\frac{j-1}{L-1} \right)^2$, where γ is the linear tilt strength and β sets a weak nonlinear term [67–69]. The nonlinear term is introduced to lift the strong degeneracies of a purely linear Stark ladder and thus restore standard level-statistics behavior. In the following we fix $\beta = 0.5$. Since the model is clean, we do not perform disorder averaging.

We first examine spectral statistics. Figure 8(a) shows the ED-based complex spacing ratio $\langle r^E \rangle$. At small γ , $\langle r^E \rangle$ is close to the Ginibre benchmark. As γ increases, $\langle r^E \rangle$ crosses over toward a GOE-like value, suggesting that the spectrum gradually becomes real and the level correlations become Hermitian-like. Upon further in-

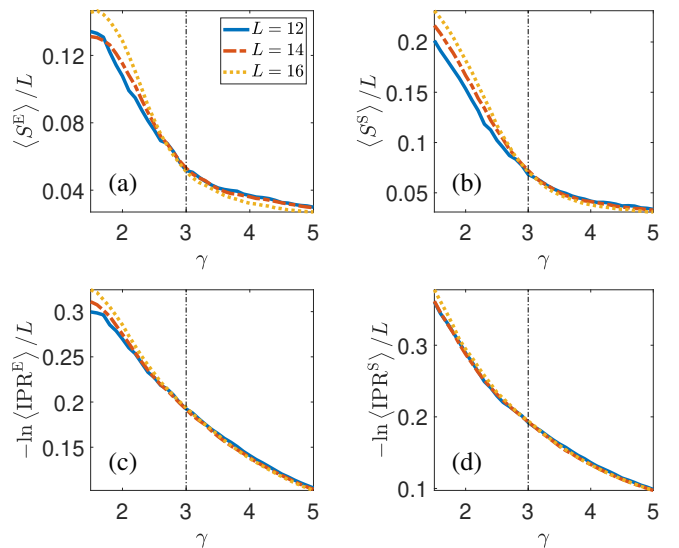


FIG. 9: Half-chain entanglement entropy and IPR versus Stark tilt γ for different system sizes. Entanglement: (a) $\langle S^E \rangle$ and (b) $\langle S^S \rangle$. IPR: (c) $\langle IPR^E \rangle$ and (d) $\langle IPR^S \rangle$. Dashed lines mark critical points from finite-size scaling.

creasing γ , $\langle r^E \rangle$ drifts toward the Poisson limit, consistent with entering an MBL-like regime. This ED sequence (Ginibre-like \rightarrow GOE-like \rightarrow Poisson-like) is consistent with the conclusion of Ref. [48]. In the SVD approach, Fig. 8(b) shows that the singular-value spacing ratio $\langle r^S \rangle$ starts near the GOE value at small γ and crosses over to the Poisson value as γ increases, indicating a transition from ergodic to MBL.

To locate the transition point, we compute eigenstate- and singular-vector-based diagnostics. Figure 9 shows the half-chain entanglement entropies $\langle S^E \rangle$ and $\langle S^S \rangle$ and the IPRs $\langle IPR^E \rangle$ and $\langle IPR^S \rangle$. The finite-size scaling collapse yields a consistent critical tilt $\gamma_c \approx 3$ as extracted from both ED and SVD, and from both entanglement and IPR. Therefore, for this clean Stark model we do not observe the systematic ED–SVD shift found in the previous two TRS-preserving disordered models.

However, this agreement should be interpreted with caution. While ED- and SVD-based diagnostics identify the transition at the same γ_c in the present Stark setting, the mechanism behind this agreement is not yet understood and calls for further investigation. In view of the pronounced ED–SVD mismatch in the quasiperiodic and random-disorder TRS-preserving models, our current conclusion is that SVD-based diagnostics cannot be regarded as a generally reliable tool to determine the MBL transition in TRS-preserving non-Hermitian systems, and ED-based diagnostics remain necessary.

V. CONCLUSION

We carried out a direct benchmark of SVD-based diagnostics against ED in TRS-preserving non-Hermitian hard-core-boson chains, using spectral statistics, eigenstate/singular-vector indicators and SSFs. For the quasiperiodic and random-disorder models, ED provides mutually consistent transition estimates from entanglement, and IPR, whereas the corresponding SVD-based estimates are systematically shifted to larger disorder strengths. This inconsistency is further reflected in the mismatch between DSFF and σ FF at the same parameters. In contrast, in the clean Stark model, ED and SVD locate the transition at a consistent tilt from both entanglement and IPR. Taken together, our results show that, in TRS-preserving non-Hermitian many-body systems, SVD-based diagnostics may reproduce the qualitative trend from RMT-like to Poisson-like behavior but are not generically reliable for quantitatively locating the MBL transition, and ED-based diagnostics remain necessary for establishing the phase boundary.

A key open question is which structural features of a TRS-preserving non-Hermitian Hamiltonian control the (dis)agreement between ED and SVD, and why the clean

Stark setting behaves differently from disordered cases. Addressing this will require systematic tests of robustness to analysis choices and scaling to larger sizes and complementary dynamical probes, in order to determine whether and when SVD can be promoted from a qualitative indicator to a quantitative tool.

Acknowledgments

Z. X. is supported by the NSFC (Grant No. 12375016) and Beijing National Laboratory for Condensed Matter Physics (No. 2023BNLCMPKF001). Y. Z. is supported by the NSFC (Grant No. 12474492 and No. 12461160324) and the Challenge Project of Nuclear Science (Grant No. TZ2025017).

Data Availability

The data that support the findings of this article are not publicly available. The data are available from the authors upon reasonable request.

[1] D. A. Abanin, E. Altman, I. Bloch, and M. Serbyn, Colloquium: Many-body localization, thermalization, and entanglement, *Rev. Mod. Phys.* **91**, 021001 (2019).

[2] D. A. Huse, Many-body localization needs a bath, *Physics* **9**, 76 (2016).

[3] V. Oganesyan and D. A. Huse, Localization of interacting fermions at high temperature, *Phys. Rev. B* **75**, 155111 (2007).

[4] R. Nandkishore and D. A. Huse, Many-body localization and thermalization in quantum statistical mechanics, *Annu. Rev. Condens. Matter Phys.* **6**, 15 (2015).

[5] J. H. Bardarson, F. Pollmann, and J. E. Moore, Unbounded growth of entanglement in models of many-body localization, *Phys. Rev. Lett.* **109**, 017202 (2012).

[6] R. Nandkishore, S. Gopalakrishnan, and D. A. Huse, Spectral features of a many-body-localized system weakly coupled to a bath, *Phys. Rev. B* **90**, 064203 (2014).

[7] S. Gopalakrishnan, K. Agarwal, E. A. Demler, D. A. Huse, and M. Knap, Griffiths effects and slow dynamics in nearly many-body localized systems, *Phys. Rev. B* **93**, 134206 (2016).

[8] J. A. Kjäll, J. H. Bardarson, and F. Pollmann, Many-body localization in a disordered quantum Ising chain, *Phys. Rev. Lett.* **113**, 107204 (2014).

[9] A. Pal and D. A. Huse, Many-body localization phase transition, *Phys. Rev. B* **82**, 174411 (2010).

[10] B. Bauer and C. Nayak, Area laws in a many-body localized state and its implications for topological order, *J. Stat. Mech.* **9**, P09005 (2013).

[11] M. Serbyn, Z. Papić, and D. A. Abanin, Universal slow growth of entanglement in interacting strongly disordered systems, *Phys. Rev. Lett.* **110**, 260601 (2013).

[12] M. Serbyn, Z. Papić, and D. A. Abanin, Local conserva-

tion laws and the structure of the many-body localized states, *Phys. Rev. Lett.* **111**, 127201 (2013).

[13] D. A. Huse, R. Nandkishore, and V. Oganesyan, Phenomenology of fully many-body-localized systems, *Phys. Rev. B* **90**, 174202 (2014).

[14] J. Dalibard, Y. Castin, and K. Mølmer, Wave-function approach to dissipative processes in quantum optics, *Phys. Rev. Lett.* **68**, 580 (1992).

[15] H. J. Carmichael, Quantum trajectory theory for cascaded open systems, *Phys. Rev. Lett.* **70**, 2273 (1993).

[16] M. B. Plenio and P. L. Knight, The quantum-jump approach to dissipative dynamics in quantum optics, *Rev. Mod. Phys.* **70**, 101 (1998).

[17] A. J. Daley, Quantum trajectories and open many-body quantum systems, *Advances in Physics* **63**, 77 (2014).

[18] Z. Gong, Y. Ashida, K. Kawabata, K. Takasan, S. Higashikawa, and M. Ueda, Topological phases of non-Hermitian systems, *Phys. Rev. X* **8**, 031079 (2018).

[19] K. Kawabata, K. Shiozaki, M. Ueda, and M. Sato, Symmetry and topology in non-Hermitian physics, *Phys. Rev. X* **9**, 041015 (2019).

[20] C. M. Bender and S. Boettcher, Real spectra in non-Hermitian Hamiltonians having PT symmetry, *Phys. Rev. Lett.* **80**, 5243 (1998).

[21] N. Hatano and D. R. Nelson, Localization transitions in non-Hermitian quantum mechanics, *Phys. Rev. Lett.* **77**, 570 (1996).

[22] I. Rotter, A non-Hermitian Hamilton operator and the physics of open quantum systems, *J. Phys. A: Math. Theor.* **42**, 153001 (2009).

[23] Y. Ashida, Z. Gong, and M. Ueda, Non-Hermitian physics, *Advances in Physics* **69**, 249 (2020).

[24] P. Nandy, T. Pathak, Z.-Y. Xian, and J. Erdmenger,

Krylov space approach to singular value decomposition in non-Hermitian systems, *Phys. Rev. B* **111**, 064203 (2025).

[25] S. H. Tekur, M. S. Santhanam, B. K. Agarwalla, and M. Kulkarni, Higher-order gap ratios of singular values in open quantum systems, *Phys. Rev. B* **110**, L241410 (2024).

[26] K. Kawabata, Z. Xiao, T. Ohtsuki, and R. Shindou, Singular-value statistics of non-Hermitian random matrices and open quantum systems, *PRX Quantum* **4**, 040312 (2023).

[27] F. Roccati, F. Balducci, R. Shir, and A. Chenu, Diagnosing non-Hermitian many-body localization and quantum chaos via singular value decomposition, *Phys. Rev. B* **109**, L140201 (2024).

[28] F. J. Dyson, Statistical theory of the energy levels of complex systems. I, *Journal of Mathematical Physics* **3**, 140 (1962).

[29] F. J. Dyson, Statistical theory of the energy levels of complex systems. II, *Journal of Mathematical Physics* **3**, 157 (1962).

[30] T. Guhr, A. Müller-Groeling, and H. A. Weidenmüller, Random-matrix theories in quantum physics: common concepts, *Physics Reports* **299**, 189 (1998).

[31] C. W. J. Beenakker, Random-matrix theory of quantum transport, *Rev. Mod. Phys.* **69**, 731 (1997).

[32] M. Prasad, S. H. Tekur, B. K. Agarwalla, and M. Kulkarni, Assessment of spectral phases of non-Hermitian quantum systems through complex and singular values, *Phys. Rev. B* **111**, L161408 (2025).

[33] M. Baggiooli, K.-B. Huh, H.-S. Jeong, X. Jiang, K.-Y. Kim, and J. F. Pedraza, Singular value decomposition and its blind spot for quantum chaos in non-Hermitian Sachdev-Ye-Kitaev models, *Phys. Rev. D* **111**, L101904 (2025).

[34] P. Nandy, T. Pathak, and M. Tezuka, Probing quantum chaos through singular-value correlations in the sparse non-Hermitian Sachdev-Ye-Kitaev model, *Phys. Rev. B* **111**, L060201 (2025).

[35] J. Sakhr and J. M. Nieminen, Spacing distributions for point processes on a regular fractal, *Phys. Rev. E* **73**, 036201 (2006).

[36] Y. Y. Atas, E. Bogomolny, O. Giraud, P. Vivo, and E. Vivo, Joint probability densities of level spacing ratios in random matrices, *J. Phys. A: Math. Theor.* **46**, 355204 (2013).

[37] Á. L. Corps and A. Relaño, Distribution of the ratio of consecutive level spacings for different symmetries and degrees of chaos, *Phys. Rev. E* **101**, 022222 (2020).

[38] S. H. Tekur, U. T. Bhosale, and M. S. Santhanam, Higher-order spacing ratios in random matrix theory and complex quantum systems, *Phys. Rev. B* **98**, 104305 (2018).

[39] P. Kumar and R. N. Bhatt, Scaling of entanglement entropy at quantum critical points in random spin chains, *Phys. Rev. B* **108**, L241113 (2023).

[40] H. Tian, T. He, and X. Wu, Finite-size scaling of half-chain entanglement entropy in the one-dimensional transverse field Ising model and the XX model, *Phys. Rev. B* **111**, 104437 (2025).

[41] P. Shukla, Disorder perturbed flat bands: Level density and inverse participation ratio, *Phys. Rev. B* **98**, 054206 (2018).

[42] F. Evers and A. D. Mirlin, Fluctuations of the inverse participation ratio at the Anderson transition, *Phys. Rev. Lett.* **84**, 3690 (2000).

[43] B. Bertini, P. Kos, and T. Prosen, Exact spectral form factor in a minimal model of many-body quantum chaos, *Phys. Rev. Lett.* **121**, 264101 (2018).

[44] Z. Wei, C. Tan, and R. Zhang, Generalized spectral form factor in random matrix theory, *Phys. Rev. E* **109**, 064208 (2024).

[45] E. Brézin and S. Hikami, Spectral form factor in a random matrix theory, *Phys. Rev. E* **55**, 4067 (1997).

[46] L.-J. Zhai, S. Yin, and G.-Y. Huang, Many-body localization in a non-Hermitian quasiperiodic system, *Phys. Rev. B* **102**, 064206 (2020).

[47] R. Hamazaki, K. Kawabata, and M. Ueda, Non-Hermitian many-body localization, *Phys. Rev. Lett.* **123**, 090603 (2019).

[48] J. Liu and Z. Xu, From ergodicity to many-body localization in a one-dimensional interacting non-Hermitian Stark system, *Phys. Rev. B* **108**, 184205 (2023).

[49] K. Suthar, Y.-C. Wang, Y.-P. Huang, H. H. Jen, and J.-S. You, Non-Hermitian many-body localization with open boundaries, *Phys. Rev. B* **106**, 064208 (2022).

[50] L. Sá, P. Ribeiro, and T. Prosen, Complex spacing ratios: A signature of dissipative quantum chaos, *Phys. Rev. X* **10**, 021019 (2020).

[51] I. I. Yusipov and M. V. Ivanchenko, Quantum Lyapunov exponents and complex spacing ratios: Two measures of dissipative quantum chaos, *Chaos: An Interdisciplinary Journal of Nonlinear Science* **32**, 043106 (2022).

[52] T. Peron, B. M. F. De Resende, F. A. Rodrigues, L. D. F. Costa, and J. A. Méndez-Bermúdez, Spacing ratio characterization of the spectra of directed random networks, *Phys. Rev. E* **102**, 062305 (2020).

[53] Y.-Y. Wang, Z.-H. Sun, and H. Fan, Stark many-body localization transitions in superconducting circuits, *Phys. Rev. B* **104**, 205122 (2021).

[54] Y. Y. Atas, E. Bogomolny, O. Giraud, and G. Roux, Distribution of the Ratio of Consecutive Level Spacings in Random Matrix Ensembles, *Phys. Rev. Lett.* **110**, 084101 (2013).

[55] G.-Q. Zhang, D.-W. Zhang, Z. Li, Z. D. Wang, and S.-L. Zhu, Statistically related many-body localization in the one-dimensional anyon Hubbard model, *Phys. Rev. B* **102**, 054204 (2020).

[56] J. Šuntajs, J. Bonča, T. Prosen, and L. Vidmar, Ergodicity breaking transition in finite disordered spin chains, *Phys. Rev. B* **102**, 064207 (2020).

[57] R. Modak and S. Mukerjee, Many-body localization in the presence of a single-particle mobility edge, *Phys. Rev. Lett.* **115**, 230401 (2015).

[58] J. Li, T. Prosen, and A. Chan, Spectral statistics of non-Hermitian matrices and dissipative quantum chaos, *Phys. Rev. Lett.* **127**, 170602 (2021).

[59] S. Ghosh, S. Gupta, and M. Kulkarni, Spectral properties of disordered interacting non-Hermitian systems, *Phys. Rev. B* **106**, 134202 (2022).

[60] F. Haake, *Quantum Signatures of Chaos* (Springer, Berlin, 2010).

[61] J. S. Cotler, G. Gur-Ari, M. Hanada, J. Polchinski, P. Saad, S. H. Shenker, D. Stanford, A. Streicher, and M. Tezuka, Black holes and random matrices, *J. High Energ. Phys.* **5**, 118 (2017).

[62] J. Liu, Spectral form factors and late time quantum

chaos, Phys. Rev. D **98**, 086026 (2018).

[63] Č. Lozej, Spectral form factor and dynamical localization, Entropy **25**, 451 (2023).

[64] M. Bianchi, M. Firrotta, J. Sonnenschein, and D. Weissman, From spectral to scattering form factor, J. High Energ. Phys. **6**, 189 (2024).

[65] J. Šuntajs, J. Bonča, T. Prosen, and L. Vidmar, Quantum chaos challenges many-body localization, Phys. Rev. E **102**, 062144 (2020).

[66] A. Prakash, J. H. Pixley, and M. Kulkarni, Universal spectral form factor for many-body localization, Phys. Rev. Research **3**, L012019 (2021).

[67] M. Schulz, C. A. Hooley, R. Moessner, and F. Pollmann, Stark many-body localization, Phys. Rev. Lett. **122**, 040606 (2019).

[68] G. H. Wannier, Dynamics of band electrons in electric and magnetic fields, Rev. Mod. Phys. **34**, 645 (1962).

[69] G. H. Wannier, Wave functions and effective Hamiltonian for Bloch electrons in an electric field, Phys. Rev. **117**, 432 (1960).